

Analytical coupled vibroacoustic modeling of membrane-type acoustic metamaterials: Plate model

Yangyang Chen^{a)} and Guoliang Huang^{a),b)}

Department of Systems Engineering, University of Arkansas at Little Rock, Little Rock, Arkansas 72204

Xiaoming Zhou and Gengkai Hu

Key Laboratory of Dynamics and Control of Flight Vehicle, Ministry of Education, School of Aerospace Engineering, Beijing Institute of Technology, Beijing 100081, China

Chin-Teh Sun

School of Aeronautics and Astronautics, Purdue University, West Lafayette, Indiana 47907

(Received 10 November 2013; revised 15 April 2014; accepted 24 October 2014)

By considering the elastic membrane's dissipation, the membrane-type acoustic metamaterial (MAM) has been demonstrated to be a super absorber for low-frequency sound. In the paper, a theoretical vibroacoustic plate model is developed to reveal the sound energy absorption mechanism within the MAM under a plane normal incidence. Based on the plate model in conjunction with the point matching method, the in-plane strain energy of the membrane due to the resonant and antiresonant motion of the attached masses can be accurately captured by solving the coupled vibroacoustic integrodifferential equation. The sound absorption ability of the MAM is quantitatively determined, which is also in good agreement with the prediction from the finite element method. In particular, microstructure effects including eccentricity of the attached masses, the depth, thickness, and loss factor of the membrane on sound absorption peak values are discussed. © 2014 Acoustical Society of America. [<http://dx.doi.org/10.1121/1.4901706>]

PACS number(s): 43.20.El, 43.20.Ks, 43.40.Dx, 43.50.Gf [ANN]

Pages: 2926–2934

I. INTRODUCTION

The attenuation/absorption of low frequency sound is of great interest for noise control. Common homogeneous materials, such as foam and composite panels, usually exhibit weak absorptions in the low frequency range, due to their dissipative power being quadratic in material velocities. Recently, membrane-type acoustic metamaterials (MAMs) have been suggested to possess excellent acoustic properties for sound insulation at the 100–1000 Hz frequency regime, the most difficult regime as dictated by the mass density law.^{1,2} This MAM comprises a pre-tensioned elastic rubber membrane attached with only one rigid circular mass. Nearly total reflection of low-frequency sound has been achieved.^{1–5} To realize broadband wave attenuation and enhance the wave dissipation, it is usually necessary to increase the energy density inside the MAM through multiple resonators. Motivated by this idea, a thin elastic membrane decorated with designed patterns of multiple rigid platelets was further suggested.⁶ The basic microstructure of this MAM consists of a membrane with multiple attached small heterogeneous masses acting as resonators with fixed boundaries imposed by a relatively rigid grid. It was reported that the one-layer of MAM can absorb 86% of the acoustic waves at ~170 Hz and can absorb 99% with two layers at the lowest resonant frequency. However, the wave

attenuation/absorption mechanism is not well interpreted and understood yet.

Issues about sound transmissions through membranes and partitions have been intensively investigated for decades.^{7–10} The classical membrane theory has been used to approximately govern the motion of the pre-stressed thin elastic membrane.¹¹ However, the dissipative/absorbed sound power, which is proportional to the total strain energy of the membrane,⁶ cannot properly be calculated by the classical membrane theory, because effects of the bending stiffness are neglected. Therefore, the flexural plate theory for the MAM will be highly needed for the purpose of the energy absorption calculation.

For vibrations of thin plates combining with various boundary conditions, governing equations and the Galerkin procedure with several approximate series solutions have been suggested.^{12,13} The problem of sound transmission through a thin plate based on vibroacoustic plate model has been solved with integrals of Green's functions.¹⁴ Whereas, modeling vibrations and sound dissipations of the MAMs would address a challenging issue, in which a pre-stressed clamped thin plate carrying finite attached masses of arbitrary shapes needs to be solved. Galerkin procedure and Rayleigh–Ritz method are the most commonly used systematic approaches to study vibrations of plates with attached masses, in which the bending stiffness of the attached mass is usually ignored.^{15,16} However, different from those studies, bending stiffness of attached masses on MAMs cannot be neglected. Instead, such attached masses would be rigid compared with the thin rubber membrane. To properly capture effects of finite masses on the small deformation of the membrane, the point matching scheme¹⁷ can be applied by

^{a)}Present address: Department of Mechanical and Aerospace Engineering, University of Missouri, Columbia, MO 65211.

^{b)}Author to whom correspondence should be addressed. Electronic mail: huangg@missouri.edu

using distributed point forces along the interfacial boundary between masses and the membrane.¹¹ Another issue about the MAM is geometric nonlinearities of the rubber membrane, in which in-plane pre-stresses are usually comparable with the Young's modulus. A plate theory considering incremental deformation and initial stress has been developed for orthotropic laminated plates.¹⁸

In this paper, to investigate sound absorptions of MAMs, we will develop a vibroacoustic plate model to accurately capture strain energy within the membrane. The initial tension effect on the effective bending stiffness of the MAM is determined by using the incremental energy method. Eigenfrequencies and eigenmodes of the MAM are solved by using point matching scheme, where the Galerkin procedure with double cosine series expansions is selected. Finally, the dissipative power is calculated through solving the coupled vibroacoustic integrodifferential equation with complex Young's modulus and the modal superposition method. Specifically, microstructure effects on sound absorptions are quantitatively investigated, which include eccentricities and numbers of masses, depth, and thickness of the membrane and the membrane's loss factor.

II. THEORETICAL PLATE MODEL

Consider now the unit cell of an MAM in a global Cartesian coordinate system (x,y) with the origin O on the lower left corner of the rectangular membrane, as shown in Fig. 1(a), where the membrane is symmetrically attached by several masses with respect to the central line of the membrane along the x direction. Masses can be of arbitrary symmetric shapes with respect to the central line of the membrane along the y direction. The number of masses is denoted as S , and there are I_s collocation points, applied with

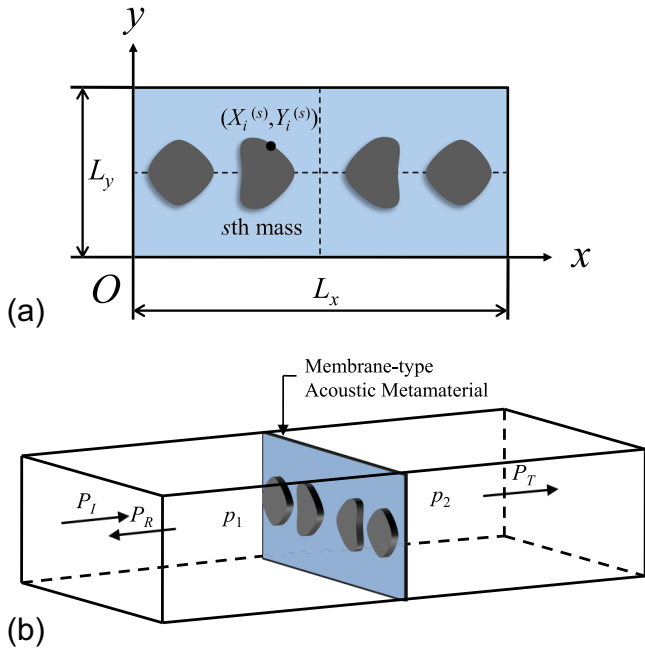


FIG. 1. (Color online) (a) The MAM symmetrically attached with multiple masses of arbitrary symmetric shapes. (b) The MAM subjected to a normal acoustic loading in a tube.

point forces along edges of the s th mass. In the figure, the membrane is subject to initial tension T per unit length uniformly in both x and y directions. The thickness, width, depth, and density per unit area of the membrane are denoted as h , L_x , L_y , and ρ_m , respectively. The i th collocation point on the inner boundaries between the s th mass and the membrane is denoted as $[X_i^{(s)}, Y_i^{(s)}]$ in the global Cartesian coordinate system (x,y) . In the study, we focus on the sound absorption of the stretched MAM in a tube subject to a normally incident plane sound wave, as shown in Fig. 1(b). Perfectly absorbing boundary conditions are assumed in both ends of the tube so that there will be no multiple reflected waves to the MAM.

A. Eigenvalue problem of the MAM

The attached masses are assumed to be rigid and perfectly bonded to the rectangular membrane. To properly capture effects of those masses on the deformation of the membrane, the point matching scheme is applied such that each mass can be represented by several point loadings on the membrane along their interfacial boundaries.¹¹ The incremental energy method is used to consider the initial stress effect, and the governing equation of the rectangular membrane can be written as

$$D^* \nabla^4 w(x, y, t) - T \nabla^2 w(x, y, t) + \rho_m \frac{\partial^2 w(x, y, t)}{\partial t^2} = \sum_{s=1}^S \sum_{i=1}^{I_s} F_i^{(s)}(t) \delta(x - X_i^{(s)}) \delta(y - Y_i^{(s)}), \quad (1)$$

where $D^* = D + (\sigma_0 h^3/12)$ is the effective bending stiffness with D and σ_0 being the bending stiffness and initial stress of the membrane, which is derived in the Appendix, $F_i^{(s)}$ in the right-hand side is the force loading at the i th collocation points from the s th attached mass along s th inner boundaries, and δ is the Dirac delta function. Since only the steady-state response field will be considered, the time factor $e^{i\omega t}$, which applies to all the field variables, will be suppressed in the paper. Then, $F_i^{(s)}$ becomes a constant to be determined. For a clamped plate, the boundary conditions are

$$w = \frac{\partial w}{\partial x} = 0, \quad \text{on } x = 0, \quad x = L_x, \quad (2)$$

$$w = \frac{\partial w}{\partial y} = 0, \quad \text{on } y = 0, \quad y = L_y. \quad (3)$$

To solve Eq. (1), the Galerkin procedure is applied to seek an approximate solution.¹³ Since a plane sound wave can only induce symmetric modes on the MAM, we choose the double cosine series expansion to satisfy boundary conditions in Eqs. (2) and (3) as^{12,13}

$$w = \sum_{m=1}^{\infty} \sum_{n=1}^{\infty} W_{mn} q_{mn}, \quad (4)$$

$$W_{mn} = \left(1 - \cos \frac{2m\pi x}{L_x}\right) \left(1 - \cos \frac{2n\pi y}{L_y}\right). \quad (5)$$

Substituting Eq. (4) into Eq. (1), multiplying each term by W_{mn} , and integrating all terms over the domain $(0 \leq x \leq L_x,$

$0 \leq y \leq L_y$), lead to a linear system of equations for q_{mn} .¹³ Solutions of q_{mn} can be expressed by the summation of $F_i^{(s)} q_{mni}^{(s)}$ from all the point loadings, where $q_{mni}^{(s)}$ is the solution of the linear system of equations with $\delta(x - X_i^{(s)}) \delta(y - Y_i^{(s)})$ in the right-hand side. Then, the solution to Eq. (1) can be expressed as

$$w = \sum_{s=1}^S \sum_{i=1}^I F_i^{(s)} Q_i^{(s)}, \quad (6)$$

where $Q_i^{(s)} = \sum_{m=1}^{\infty} \sum_{n=1}^{\infty} q_{mni}^{(s)} [1 - \cos(2m\pi x/L_x)][1 - \cos(2n\pi y/L_y)]$.

The unknown loading $F_i^{(s)}$ can be determined through the inner boundary conditions between the membrane and masses. The natural frequencies and mode shape functions of the MAM can be determined by using the same techniques in Ref. 11.

B. Vibroacoustic modeling of the MAM

Consider a plane sound wave is normally incident on the MAM. According to the fact that the thickness of the MAM is extremely small compared with the wavelength of low-frequency sound in air, thickness effects of the MAM can be ignored. The objective is to determine the dissipated power within the MAM. The governing equation of the acoustic excited membrane based on the plate theory can be expressed as

$$\begin{aligned} D^* \nabla^4 w - T \nabla^2 w - \omega^2 \rho_m w \\ = p_1|_{(z=0)} - p_2|_{(z=0)} + \sum_{s=1}^S \sum_{i=1}^{I_s} F_i^{(s)} \delta(x - X_i^{(s)}) \delta(y - Y_i^{(s)}), \end{aligned} \quad (7)$$

where p_1 and p_2 are pressures on the left and right surfaces of the MAM. It should be noted that damping effects in forced vibration analyses are considered by assuming the Young's modulus of the membrane to be a complex number. Then, D^* is a complex number in Eq. (7).

By combining equations in the acoustic field,¹¹ Eq. (7) can be rewritten as

$$\begin{aligned} D^* \nabla^4 w - T \nabla^2 w - \omega^2 \rho_m w + 2i\omega \rho_a c_a \langle w \rangle \\ - 2\omega^2 \rho_a \int_0^{L_x} \int_0^{L_y} G \delta w dx^* dy^* \\ = 2P_I + \sum_{s=1}^S \sum_{i=1}^{I_s} F_i^{(s)} \delta(x - X_i^{(s)}) \delta(y - Y_i^{(s)}), \end{aligned} \quad (8)$$

in which the Green function $G = e^{ik_a S} / 4\pi S + e^{ik_a S_1} / 4\pi S_1$ with $S = \sqrt{(x - x^*)^2 + (y - y^*)^2 + (z - z^*)^2}$, $S_1 = \sqrt{(x - x^*)^2 + (y - y^*)^2 + (z + z^*)^2}$; $\langle \cdot \rangle$ denotes the average of the parameter; $\delta w = w - \langle w \rangle$; ρ_a , c_a , and k_a are the density of air, sound speed, and wave number of acoustic waves in air, respectively. The displacement field in Eq. (8) can then be solved by modal superposition method.¹¹

For the application of the MAM, the acoustic wavelength (λ) for low frequency sound (50 to 1000 Hz) is usually much larger than the dimension of the membrane ($\lambda \gg L_x, L_y$). According to Ref. 11, the higher order scattered waves are caused by the deviation of the out-of-plane displacement, and the longest wavelength along lateral direction is $(\lambda_{\parallel})_{\max} = (L_x, L_y)_{\max}$. Consequently, the lateral component of the wave number of higher order scattered waves, $k_{\parallel} = 2\pi/L_x$, would be much greater than the maximum total wave number, $(k_a)_{\max} = \omega_{\max}/c_a$. As a result, the normal component of the wave number (along the z direction) of higher order scattered waves, $k_z = \sqrt{k_a^2 - k_{\parallel}^2}$, is always an imaginary number. Therefore, the higher order scattered waves are eventually evanescent waves because the normal (z) component of wave number is an imaginary number, and their amplitude will decay exponentially along the normal (z) direction.

Therefore, the far field transmission and reflection coefficients for radiated plane waves of the MAM can be expressed as¹¹

$$\tilde{T} = \frac{P_T}{P_I} = \frac{i\omega \rho_a c_a \langle w \rangle}{P_I}, \quad (9)$$

$$\tilde{R} = \frac{P_R}{P_I}, \quad (10)$$

with the relation being

$$\tilde{R} = 1 - \tilde{T}, \quad (11)$$

with P_I , P_R , and P_T being complex amplitudes of incident, reflected, and transmitted plane waves.

The intensity transmission and reflection coefficients are¹¹

$$T_I = |\tilde{T}|^2, \quad (12)$$

$$R_I = |\tilde{R}|^2. \quad (13)$$

Therefore, the dissipated power of the MAM can be calculated as

$$A_I = 1 - T_I - R_I = 2(\text{Re}(\tilde{T}) - \text{Re}(\tilde{T})^2 - \text{Im}(\tilde{T})^2), \quad (14)$$

where $|\text{Re}(\tilde{T})| \leq 1$ and $|\text{Im}(\tilde{T})| \leq 1$ according to the definition of acoustic transmission and reflection coefficients. Therefore, it can be easily derived that the maximum dissipated power A_I cannot be greater than 50% for any thin MAM. It is noted that the air viscosity for the energy absorption are not taken into account in the current model.

III. VALIDATION OF THE THEORETICAL MODELING

To verify the developed vibroacoustic plate model, acoustic and vibration properties of the MAM from the current model are compared with those from the commercial finite element software, COMSOL Multiphysics, in which the acoustic-solid interaction with geometric nonlinearities is selected. The MAM consists of a membrane

symmetrically attached with two semicircular platelets, as shown in Fig. 2. It is sandwiched between two air blocks. Fixed boundary conditions are applied on all edge surfaces of the membrane, and the rigid wall boundary condition is used for the side boundary of the air. Two acoustic radiation boundaries are assumed on both ends of the system. A plane incident wave is applied on the left end of the tube. Acoustic-structure interface boundaries are selected on the MAM. The elements used for the system are 3-D solid elements. Transmitted pressure is calculated by averaging the surface pressure on the right end of the system, and reflected pressure is calculated by subtracting the incident pressure from the average of the surface pressure on the left end of the system. The intensity coefficients and absorptions of the MAM can then be obtained from Eqs. (9)–(14). Material properties and geometrical dimensions of the membrane and attached masses are given in Table I. The loss factor of the rubber is set to be $\chi_0\omega$ with $\chi_0 = 4.2 \times 10^{-4}$ s. For properties of air, $\rho_1 = 1.29 \text{ kg/m}^3$ and $c_1 = 340 \text{ m/s}$. The convergence of the finite element analysis is first conducted through analysis of absorption coefficients and displacement amplitudes at the first absorption peak frequency with different meshes, as shown in Figs. 3(a) and 3(b), respectively. It can be found that the numerical results are convergent when the number of total degree of freedoms (DOFs) of the system approaches 600 thousands.

Figure 4 shows the comparison of intensity transmission, reflection, and absorption coefficients of the MAM from both the theoretical model, the finite element analysis and the experiment by Mei *et al.*⁶ (absorption only). For the metamaterial device application, we also calculated the sound absorption of an MAM panel composed with four unit cells based on the finite element simulation. In the theoretical model, the number of collocation points for one half of the semicircular mass is set as $l = 20$, and the number of cosine series expansions are truncated as $M = N = 40$ to make the result convergent. It can be seen that our analytical results (solid line) agree well with those from the finite element method (dash line). Three absorption peaks, located in 190, 356, and 727 Hz from the analytical model and 190, 344, and 710 Hz from the finite element method, together with three transmission peaks are observed near resonant frequencies, which are 189, 356, and 733 Hz from the analytical

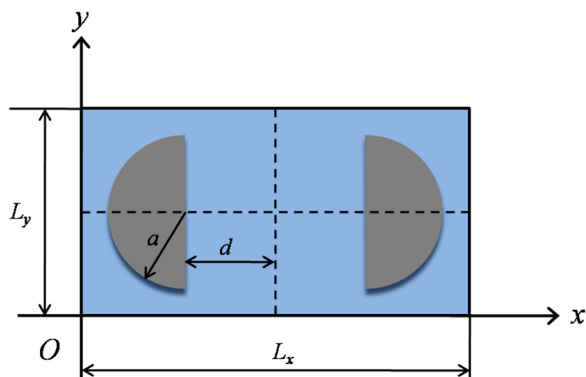


FIG. 2. (Color online) The MAM symmetrically attached with two semicircular masses.

TABLE I. Material properties and geometric parameters (2 masses).

	Membrane	Mass
Mass Density (kg/m^3)	980	7870
Young's modulus (Pa)	1.9×10^6	2×10^{11}
Poisson ratio	0.48	0.30
Thickness (mm)	0.2	1
Width (mm)	31	-
Height (mm)	15	-
Radius (mm)	-	6
Eccentricity d (mm)	-	7.5
Pretension (N/m)	44.0	0

model and 191, 337, and 738 Hz from the finite element method. The three transmission peaks are due to the resonant motion of the MAM at three lowest symmetric modes, while two transmission dips are caused by the antiresonant motion of the MAM. Based on discussions in Ref. 11, the sound transmission is proportional to the averaged velocity of the membrane. The dissipated power (absorption coefficient) at the three absorption peaks is calculated to be 37%, 31%, and 26% from the theoretical model and 41%, 22%, and 29% from the finite element method. In addition, it is worth noticing that acoustic absorption of the MAM with multi-celled partitions is almost the same as those predicted from the MAM with a single cell. Therefore, the developed

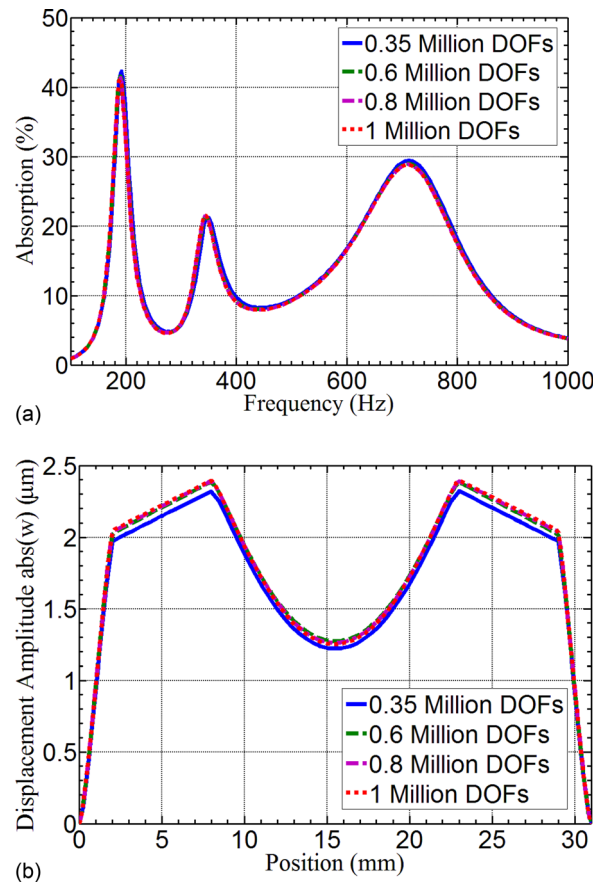


FIG. 3. (Color online) (a) Convergence analysis of the finite element method: Absorption coefficient. (b) Convergence analysis of the finite element method: Displacement amplitudes at the first absorption peak frequency.

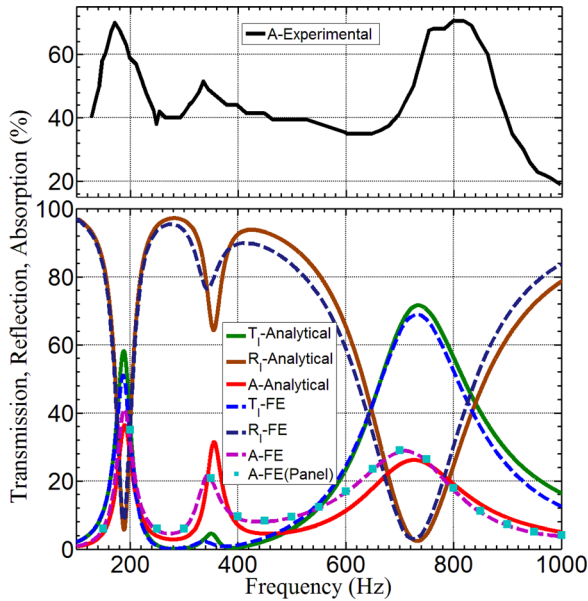


FIG. 4. (Color online) Comparison of intensity transmission, reflection and absorption coefficients of the MAM with two semicircular masses between analytical, finite element (one unit cell and four unit cell panel) and experimental results (absorption only).

theoretical model can be applied for the vibroacoustic analysis of the metamaterial device with multi-cells.

The loss factor is usually determined by fitting theoretical absorptions with experimental absorptions. Effects of loss factors will be discussed in the next section. However, as illustrated in Eq. (14), dissipations would not be greater than 50% with any loss factors. The comparison of wave absorption predicted from theoretical model, finite element method, and experimental measurements is added in Fig. 4. The main trend of the experimental measurement is almost the same as those from theoretical model and finite element simulations. For example, the frequencies of the three sound

absorption peaks predicted from the theoretical model and experimental testing are in very good agreement. However, difference of wave absorption magnitude prediction of the metamaterial from the theoretical model and experimental testing can also be obviously observed, which needs to be studied further. The difference may be attributed to the following two facts. First, the higher experimentally measured sound absorption could be caused by multi-reflections between the sound speaker and the MAM in the left tube, which is not considered in the current model. Another reason of the higher sound absorption in the experiment could be the imperfect symmetry of attached masses, which can excite asymmetric modes. However, these asymmetric-induced modes are not taken into account in both the analytical model and the finite element method.

To validate the capacity of the current model for the energy absorption, the displacement amplitude and strain energy density within the mid-plane of the membrane at three absorption peak frequencies predicted from the current model and the finite element method are compared at Fig. 5 and Fig. 6. The images in Fig. 5(a) and Fig. 6(a) are from the analytical model, and the images in Fig. 5(b) and Fig. 6(b) are from the finite element method. The strain energy density within the mid-plane of the membrane in the 2-D theoretical model is calculated by averaging the strain energy density within the plate through the thickness. The color bar in the figure represents a logarithmic scale for the strain energy density. Good agreement between the analytical and numerical results is observed in both Figs. 5 and 6. As shown in Fig. 5, for the MAM with two attached semicircular masses, the first absorption peak is caused by both the translational and rotational motion of the masses, whereas the second peak is mainly caused by the rotational motion of the masses. The third peak is caused by the strong vibration of the partial membrane between the two masses. From Fig. 6, it can be seen that the strain energy density in the perimeter

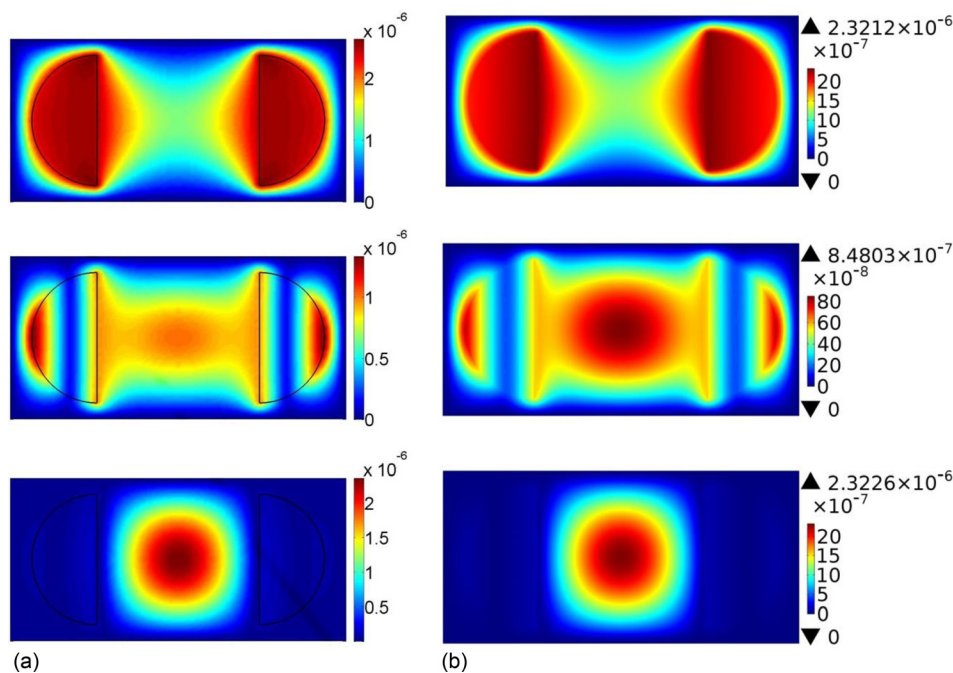


FIG. 5. (Color online) Validation of displacement amplitude at absorption peak frequencies of the MAM with two semicircular masses.

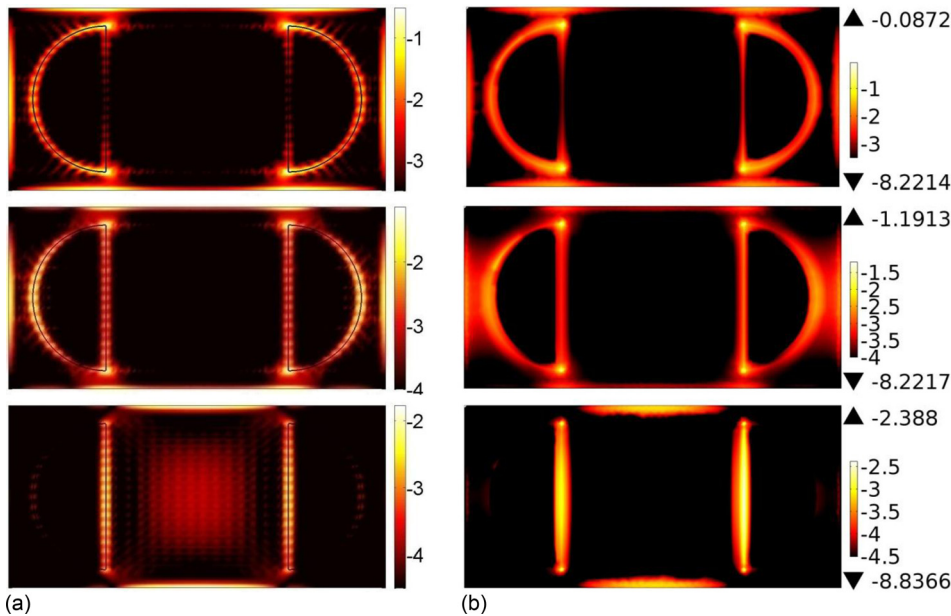


FIG. 6. (Color online) Validation of strain energy density at absorption peak frequencies of the MAM with two semicircular masses.

and clamped regions of the membrane is extremely much higher than the other regions by about three orders of magnitude at all the three absorption peaks. According to the fact that the local dissipated power is proportional to the strain energy density, most of the absorbed sound energy would be dissipated in these regions. The largest absolute discrepancy (around 10%) of the absorption at the second peak can be attributed to the approximation of the Kirchhoff hypothesis, which assumes that in-plane shear strains are dependent on out-of-plane displacement. Overall, it is clearly evident that the proposed model can accurately capture the sound energy dissipation behavior of the MAM as those in the finite element method.

IV. RESULTS AND DISCUSSIONS

Based on the developed analytical model, we will investigate effects of the eccentricity of masses, the width and thickness of the membrane and loss factors on the sound absorption behavior of the above MAM. The MAM attached with multiple semicircular masses will be also considered. The purpose of this study is to develop an accurate and highly effective analytical tool to optimize the design of MAMs on sound dissipations.

A. The MAM with two semicircular masses

In practice, eccentricity of attached masses is a critical parameter that can be easily changed to fulfill design requirement of an MAM. Figure 7 shows effects of eccentricities of two symmetric semicircular masses on sound absorptions of the MAM. In the figure, the material and geometric properties of the MAM are the same as listed in Table I with $\chi_0 = 4.2 \times 10^{-4}$ s, and only the eccentricity of attached masses is changed. It can be found that the first absorption peak value is increased with the increase of the eccentricity. However, the third absorption peak value is decreased with the increase of the eccentricity. It is understandable that when the eccentricity is increased, the membrane curvature

around circular edges of attached masses and two vertically clamped edges will become larger at the first resonant frequency, where masses vibrate strongly with both translational and rotational motion. The strain energy density in these regions will then become higher, therefore, the total absorption will increase at the first resonance frequency. The decrease of the third peak is caused by the reduced membrane curvature along straight edges of masses, in which the highest strain energy density concentrates by a strong vibration of the membrane. The second peak is increased slightly, when d is changed from 6.5 to 7.5 mm, and is reduced from 31% to 18%, when d is changed from 7.5 to 8.5 mm. The sharp drop of the second peak is due to the decrease of rotational displacement amplitudes of attached masses and membrane curvatures in parameter regions. It should be mentioned that the eccentricity can also affect the resonant frequencies of the MAM.

The membrane's width effects on sound absorption of the MAM are illustrated in Fig. 8. In the figure, the material and geometric properties of the MAM are the same as listed in Table I with $\chi_0 = 4.2 \times 10^{-4}$ s, and only the width of the

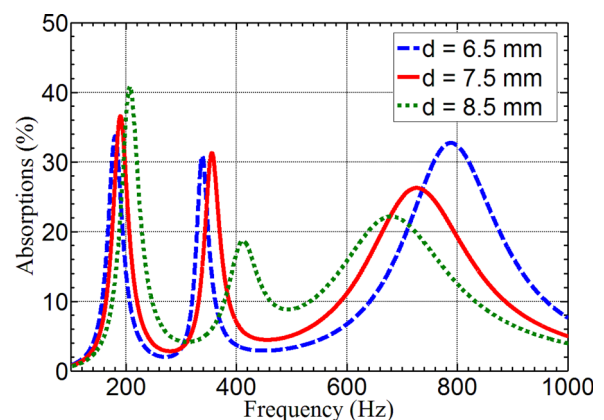


FIG. 7. (Color online) Effects of masses' eccentricities to sound absorption of the MAM with two semicircular masses.

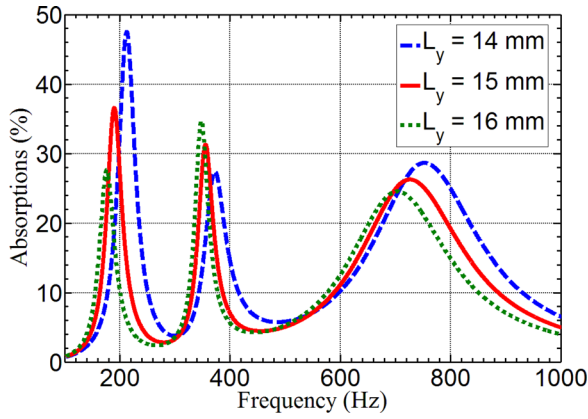


FIG. 8. (Color online) Effects of membrane's width to sound absorption of the MAM with two semicircular masses.

membrane is changed. As shown in the figure, when the width is reduced from 16 to 14 mm, the first absorption peak is raised from 28% to 47%, and the third peak is increased from 25% to 29%, whereas the second peak is decreased from 34% to 27%. All of the three resonant frequencies will also be increased slightly. The increased absorption values at the first and third resonant frequencies are caused by the increased curvature in sharp corners of masses. The decreased absorption is due to the reduced rotational displacement amplitudes of attached masses at the second resonant frequency.

Figure 9 shows effects of membrane's thickness on sound absorption of the MAM. In the figure, the material and geometric properties of the AM are the same as listed in Table I with $\chi_0 = 4.2 \times 10^{-4}$ s, only the thickness of the membrane is changed. It can be seen that the first and third sound absorption peaks are increased when the membrane becomes thicker. The second sound absorption peak, however, is reduced. The increased absorptions can be attributed to the increase of the bending stiffness of the plate, which is proportional to the strain energy density of the plate. Nevertheless, the thicker membrane would confine rotational motion of attached masses, and eventually the sound absorption of the MAM will be reduced at the second resonant frequency.

Figure 10 illustrates effects of χ_0 , a constant of the loss factor, on sound absorption of the MAM. In the figure,

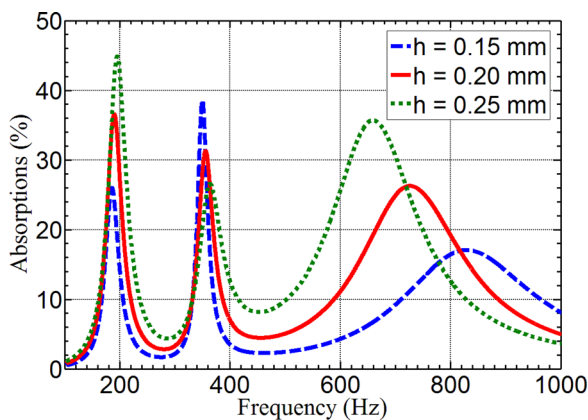


FIG. 9. (Color online) Effects of membrane's thickness to sound absorption of the MAM with two semicircular masses.

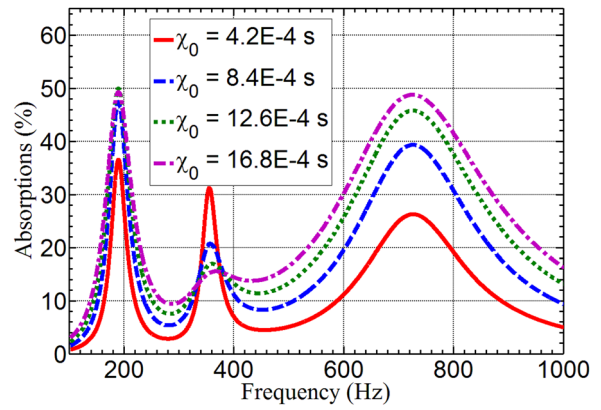


FIG. 10. (Color online) Effects of membrane's loss factors to sound absorption of the MAM with two semicircular masses.

material and geometric properties of the MAM are the same as listed in Table I, only χ_0 is changed. It can be easily observed that the 50% limit of sound absorption of the MAM is further verified numerically. As expected, absorption at most of the frequency range can be increased by raising the value of χ_0 , until the absorption reaches its limit. It is understandable that the larger loss factor usually means more energy can be damped and absorbed within the membrane. However, when the dissipated power has reached the limit with the increase of χ_0 , it cannot be increased anymore, and it will be decreased instead with the increase of χ_0 .

B. The MAM with four semicircular masses

Sound absorption of the MAM attached with four semicircular masses, as shown in Fig. 11, are investigated by the developed vibroacoustic plate model. In the figure, the eccentricities of inner and outer masses, d_1 and d_2 and the length of the membrane are selected as 7.5, 16.5, and 49.0 mm, respectively. Other material and geometric properties of the MAM are the same as listed in Table I. Sound absorptions of the MAM are plotted in Fig. 12 in function of χ_0 . When four attached masses are used, two additional absorption peaks are obviously observed for $\chi_0 = 2.1 \times 10^{-4}$ s. It should be mentioned that the second peak becomes less distinct when χ_0 is above 4.2×10^{-4} s. Effects of χ_0 on the other peaks are similar as those of the MAM with two attached masses. The displacement amplitude fields in the MAM at the five peak frequencies are shown in Fig. 13. It can be found that the first four absorption peaks of the MAM are caused by both translational and

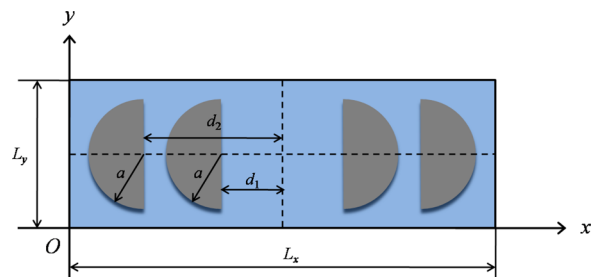


FIG. 11. (Color online) The MAM symmetrically attached with four semicircular masses.

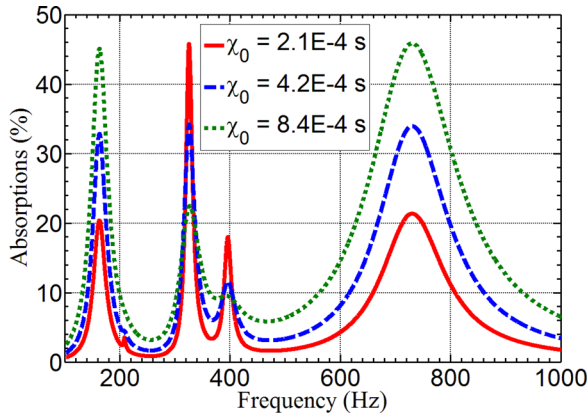


FIG. 12. (Color online) Sound absorption of the MAM with four semicircular masses with different loss factors.

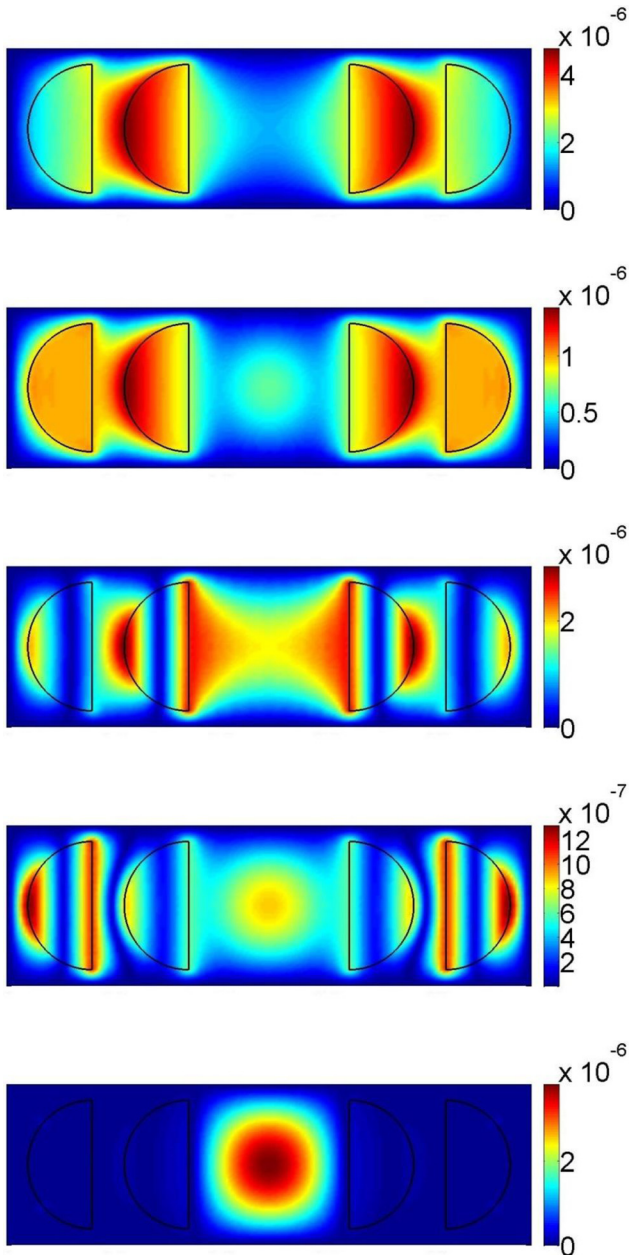


FIG. 13. (Color online) Displacement amplitude at absorption peak frequencies of the MAM with four semicircular masses.

rotational motions of the attached masses, whereby the fifth absorption peak is caused by a strong vibration of the membrane. It can be concluded that the more masses the MAM attached, the more resonant frequencies can be found in the low frequency range, which can produce more sound absorption peaks and make the spectrum of sound absorptions broader eventually.

V. CONCLUSIONS

The vibroacoustic plate model is first developed to study sound absorptions and energy dissipations within MAMs under a normal incidence. The incremental energy method is applied to derive the effective bending stiffness of plates with initial in-plane stresses. Based on the plate model in conjunction with the point matching method, the in-plane strain energy of the membrane due to the resonant and anti-resonant motion of the attached masses can be accurately captured by solving the coupled vibroacoustic integrodifferential equation. Therefore, the sound absorption of the MAM is obtained and discussed. The accuracy of the model is verified by comparison with the finite element method. Finally, parameter studies including masses' eccentricities and the width, thickness and the loss factor of the membrane on the sound absorption behaviors of the MAM with multiple attached masses are initially demonstrated.

ACKNOWLEDGMENTS

The authors would like to thank Dr. Ping Sheng from Hong Kong University of Science and Technology and Dr. Jun Mei from South China University of Technology for their comments and discussions. This work was supported in part by the Air Force Office of Scientific Research under Grant No. AF 9550-10-0061 with Program Manager Dr. Byung-Lip (Les) Lee, the National Science Foundation under award No. EPS-1003970, and by National Natural Science Foundation of China under Grants 11221202, 11290153, and 11172038.

APPENDIX: EFFECTIVE BENDING STIFFNESS OF THE PLATE WITH INITIAL STRESS

The flexural motion of a pre-tensioned elastic rubber membrane is described by a thin plate model with uniform in-plane initial stress, $\sigma_0 = T/h$, in both x and y directions, and the magnitude of initial stresses are comparable with the Young's modulus of the rubber membrane. According to the Kirchhoff hypothesis,¹³ displacement fields in x and y directions can be expressed, respectively, as

$$u(x, y, z, t) = -z \frac{\partial w(x, y, t)}{\partial x}, \quad (\text{A1})$$

$$v(x, y, z, t) = -z \frac{\partial w(x, y, t)}{\partial y}, \quad (\text{A2})$$

where z denotes the coordinate measured from the neutral plane of the membrane, and w is the out-of-plane displacement of this neutral plane. Green-Lagrangian in-plane strains are considered and expressed by¹⁸

$$\varepsilon_x = -z \frac{\partial^2 w}{\partial x^2} + \frac{1}{2} \left[\left(z \frac{\partial^2 w}{\partial x^2} \right)^2 + \left(z \frac{\partial^2 w}{\partial x \partial y} \right)^2 + \left(\frac{\partial w}{\partial x} \right)^2 \right], \quad (\text{A3})$$

$$\varepsilon_y = -z \frac{\partial^2 w}{\partial y^2} + \frac{1}{2} \left[\left(z \frac{\partial^2 w}{\partial y^2} \right)^2 + \left(z \frac{\partial^2 w}{\partial x \partial y} \right)^2 + \left(\frac{\partial w}{\partial y} \right)^2 \right], \quad (\text{A4})$$

$$\varepsilon_{xy} = -z \frac{\partial^2 w}{\partial x \partial y} + \frac{1}{2} \left[z^2 \frac{\partial^2 w}{\partial x^2} \frac{\partial^2 w}{\partial x \partial y} + z^2 \frac{\partial^2 w}{\partial y^2} \frac{\partial^2 w}{\partial x \partial y} + \frac{\partial w}{\partial x} \frac{\partial w}{\partial y} \right]. \quad (\text{A5})$$

The out-of-plane shear strains and stresses are neglected. Because of the free surfaces of the plate, we have $\sigma_z = 0$. If we assume the incremental deformation is infinitesimal, the final state of stress can be given by the Trefftz stress components as^{18,19}

$$\sigma_x = \sigma_0 + \frac{E}{(1-\nu^2)} (\varepsilon_x + \nu \varepsilon_y), \quad (\text{A6})$$

$$\sigma_y = \sigma_0 + \frac{E}{(1-\nu^2)} (\varepsilon_y + \nu \varepsilon_x), \quad (\text{A7})$$

$$\sigma_{xy} = G \varepsilon_{xy}, \quad (\text{A8})$$

in which $G = E/2(1+\nu)$ with E and ν being the Young's modulus and Poisson's ratio of the stretched elastic membrane.

Based on the linear constitutive relation in Eqs. (A6)–(A8), the strain energy per unit initial volume is¹³

$$PE = \sigma_0 (\varepsilon_x + \varepsilon_y) + \frac{E}{2(1-\nu^2)} \left[\varepsilon_x^2 + \varepsilon_y^2 + 2\nu \varepsilon_x \varepsilon_y + 2(1-\nu) \varepsilon_{xy}^2 \right]. \quad (\text{A9})$$

The incremental strain energy is

$$\Delta PE = PE - \sigma_0 (\bar{\varepsilon}_x + \bar{\varepsilon}_y), \quad (\text{A10})$$

where $\bar{\varepsilon}_x = \partial u / \partial x$ and $\bar{\varepsilon}_y = \partial v / \partial y$ are usual linear strains.¹⁹

Substituting Eqs. (A3)–(A5) and Eq. (A9) into Eq. (A10), the total incremental strain energy per unit initial area can be obtained by integrating ΔPE over the plate thickness and neglecting terms with three or higher order powers in displacement-gradients as

$$U = \frac{1}{2} \left\{ \frac{\sigma_0 h^3}{12} \left[\left(\frac{\partial^2 w}{\partial x^2} \right)^2 + \left(\frac{\partial^2 w}{\partial y^2} \right)^2 + 2 \left(\frac{\partial^2 w}{\partial x \partial y} \right)^2 \right] + T \left[\left(\frac{\partial w}{\partial x} \right)^2 + \left(\frac{\partial w}{\partial y} \right)^2 \right] + D \left\{ (\nabla^2 w)^2 - 2(1-\nu) \left[\frac{\partial^2 w}{\partial x^2} \frac{\partial^2 w}{\partial y^2} - \left(\frac{\partial^2 w}{\partial x \partial y} \right)^2 \right] \right\} \right\}, \quad (\text{A11})$$

in which $D = Eh^3/[12(1-\nu^2)]$. The kinetic energy per unit initial area of the membrane is expressed as¹⁸

$$K = \frac{1}{2} \rho_m \left(\frac{\partial w}{\partial t} \right)^2. \quad (\text{A12})$$

By applying Hamilton's principle on Eq. (A11) and Eq. (A12), the governing equation of flexural motion of pre-stressed plate can be written as

$$D^* \nabla^4 w - T \nabla^2 w + \rho_m \frac{\partial^2 w}{\partial t^2} = 0, \quad (\text{A13})$$

where $\nabla^4 = \nabla^2(\nabla^2)$, $\nabla^2 = (\partial^2/\partial x^2) + (\partial^2/\partial y^2)$, and $D^* = D + (\sigma_0 h^3/12)$, which is the effective bending stiffness of the plate.

¹Z. Yang, J. Mei, M. Yang, N. H. Chan, and P. Sheng, "Membrane-type acoustic metamaterial with negative dynamic mass," *Phys. Rev. Lett.* **101**, 204301 (2008).

²Z. Yang, H. M. Dai, N. H. Chan, G. C. Ma, and P. Sheng "Acoustic metamaterial panels for sound attenuation in the 50-1000Hz regime," *Appl. Phys. Lett.* **96**, 041906 (2010).

³C. J. Naify, C. M. Chang, G. McKnight, F. Scheulen, and S. Nutt, "Membrane-type metamaterials: Transmission loss of multi-celled arrays," *J. Appl. Phys.* **109**, 104902 (2011).

⁴C. J. Naify, C. M. Chang, G. McKnight, and S. Nutt, "Transmission loss of membrane-type acoustic metamaterials with coaxial ring masses," *J. Appl. Phys.* **110**, 124903 (2011).

⁵C. J. Naify, C. M. Chang, G. McKnight, and S. Nutt, "Scaling of membrane-type locally resonant acoustic metamaterial arrays," *J. Acoust. Soc. Am.* **132**(4), 2784–2792 (2012).

⁶J. Mei, G. C. Ma, M. Yang, Z. Yang, W. J. Wen, and P. Sheng, "Dark acoustic metamaterials as super absorbers for low-frequency sound," *Nat. Commun.* **3**, 756 (2012).

⁷P. M. Morse, *Vibration and Sound*, 2nd ed. (McGraw-Hill, New York, 1948), pp. 200–203.

⁸N. Romilly, "Transmission of sound through a stretched ideal membrane," *J. Acoust. Soc. Am.* **36**(6), 1104–1109 (1964).

⁹D. S. Ahluwalia, G. A. Kriegsmann, and E. L. Reiss, "Scattering of low-frequency acoustic waves by baffled membranes and plates," *J. Acoust. Soc. Am.* **78**(2), 682–687 (1985).

¹⁰F. J. Fahy and P. Gardonio, *Sound and Structural Vibration-Radiation, Transmission and Response* (Academic, The Netherlands, 2007), Chap. 5.

¹¹Y. Y. Chen, G. L. Huang, X. M. Zhou, G. K. Hu, and C. T. Sun, "Analytical coupled vibroacoustic modeling of membrane-type acoustic metamaterials: Membrane model," *J. Acoust. Soc. Am.* **136**(3), 969–979 (2014).

¹²A. W. Leissa, "Vibrations of plates," NASA Report No. SP-160, National Aeronautics and Space Administration, Washington, DC (1969).

¹³A. W. Leissa and M. S. Qaut, *Vibration of Continuous Systems* (McGraw-Hill, New York, 2011), pp. 221–267.

¹⁴J. E. Young, "Transmission of sound through thin elastic plates," *J. Acoust. Soc. Am.* **26**(4), 485–492 (1954).

¹⁵O. Kopmaz and S. Telli, "Free vibrations of a rectangular plate carrying a distributed-mass," *J. Sound Vib.* **251**(1), 39–57 (2002).

¹⁶Z. M. Wu, X. H. Ma, P. N. Brett, and J. W. Xu, "Vibration analysis of submerged rectangular microplates with distributed mass loading," *Proc. R. Soc. A* **465**, 1323 (2009).

¹⁷K. Nagaya and K. Poltorak, "Method for solving eigenvalue problems of the Helmholtz equation with a circular outer and a number of eccentric circular inner boundaries," *J. Acoust. Soc. Am.* **85**(2), 576–581 (1989).

¹⁸C. T. Sun, "Incremental deformations in orthotropic laminated plates under initial stress," *J. Appl. Mech.* **40**(1), 193–200 (1973).

¹⁹F. Song, G. L. Huang, H. S. Park, and X. N. Liu, "A continuum model for the mechanical behavior of nanowires including surface and surface-induced initial stresses," *Int. J. Solids Struct.* **48**, 2154–2163 (2011).